Supporting Information

In operando charge transport imaging of atomically thin dopant nanostructures in silicon

Alexander Kölker,*[a] Georg Gramse, [b,d] Taylor J. Z. Stock, [a] Gabriel Aeppli [e,f,g] and Neil J. Curson [a,c]

a. London Centre of Nanotechnology, UCL, 17-19 Gordon Street, London WC1H 0AH, UK
b. Johannes Kepler University, Biophysics Institute, Gruberstrasse 40, 4020 Linz, Austria
c. Department of Electronic and Electrical Engineering, UCL, Torrington Place, London, WC1E 7JE, UK
d. Keysight Laboratories, Keysight Technologies, Inc., Gruberstrasse 40, 4020 Linz, Austria
e. Department of Physics and Quantum Center, ETH, Zurich CH-8093 Switzerland
f. Institut de Physique, EPFL, Lausanne CH-1015, Switzerland
g. Paul Scherrer Institut, Villigen CH-5232, Switzerland

Device Fabrication

The dimensions of the phosphorus (P) wire (1 µm x 10 µm) and contact pads (2 µm x 3 µm) – see Figure S1 - were chosen such that an AFM tip can be conveniently approached to the active wire region between the source (S) and drain (D) contacts. With these dimensions, the cross-talk between Al contacts and tip is minimised when scanning under changing bias condition. This enables characterisation of the wire properties without perturbations arising from the contacts.

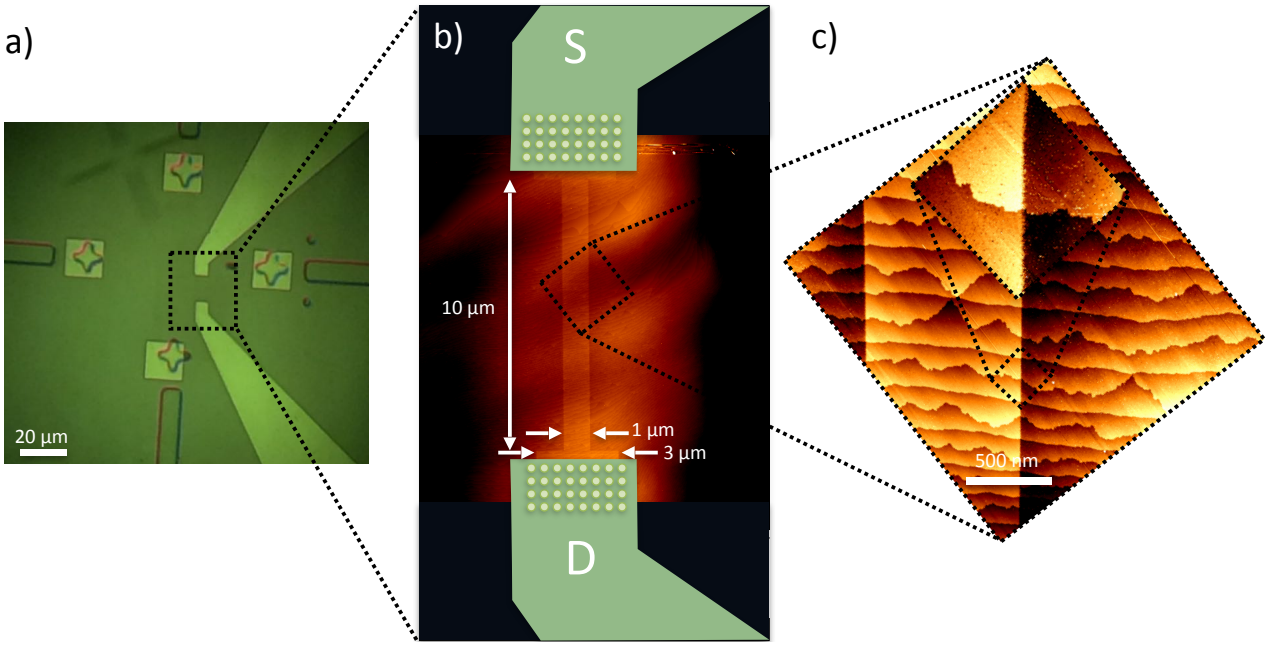

Figure S1: Sample design of the buried P nanowire. a) Micrograph of the active device area showing alignment markers and source (S) and drain (D) leads. b) STM filled states topography image (U = -2 V, I = 20 pA) of the patterned wire structure after hydrogen depassivation (depassivation parameters: U_{lith} = 8 V, I = 2 nA, 100 nm/s), overlaid with a schematic of source S and D Al contacts (green). The array of circles shows the position where vias are etched into the silicon to facilitate contact between the deposited Al and the buried P contact pads. c) STM filled state topography image of the middle wire region after depassivation, displaying flat terraces of silicon separated by single atom-high step edges, confirming a complete H-desorption within the depassivated area.

STM filled states topography images in Figure S2a-c show a successful complete depassivation over the whole length of the patterned region. The depassivation process for such a large structure took ~20 h. After

PH_3 exposure, a magnified area of the edge of the middle region of the wire (dashed white region in Figure S2b) reveals PH_3 adsorption exclusively within the depassivated region, see Figure S2d and magnified area in Figure S2e.

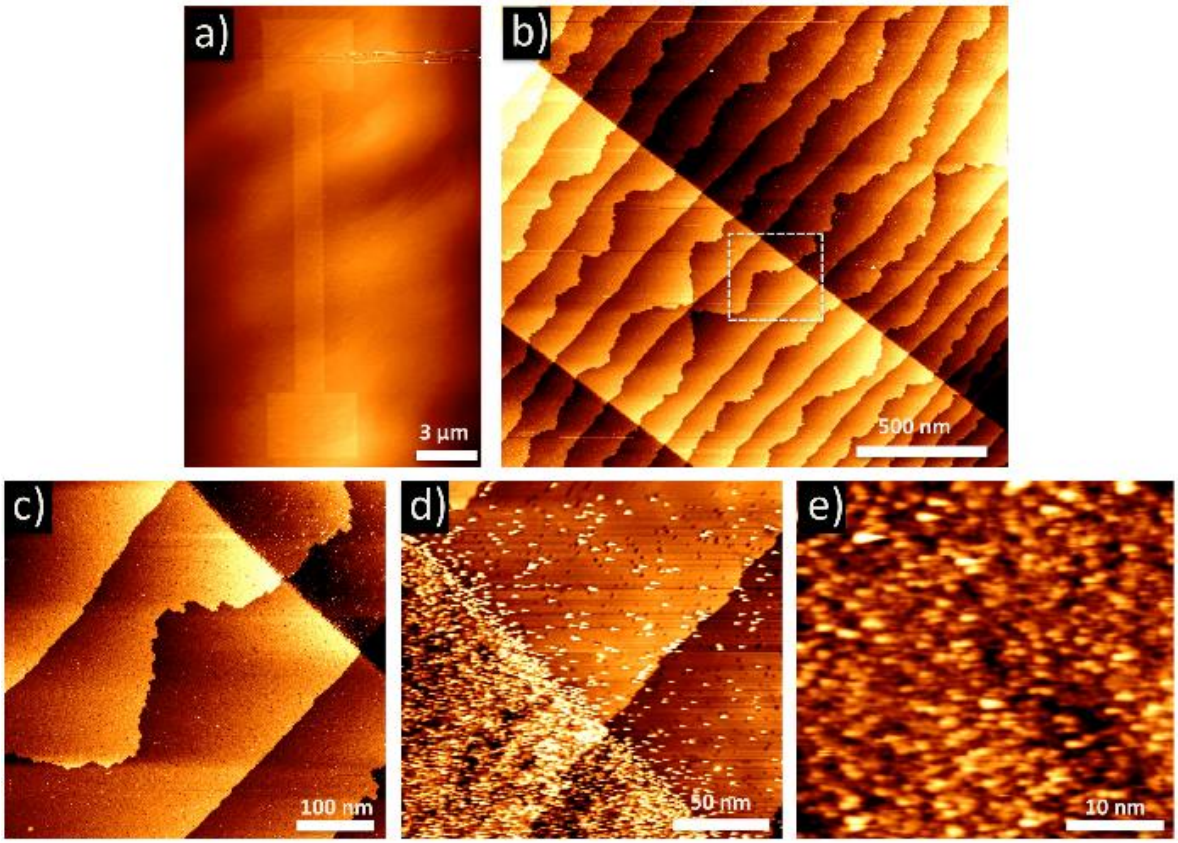

Figure S2: STM filled state topography images of the buried P nanowire structure. a)-c) Demonstrate complete depassivation of a region of clean hydrogen terminated silicon in the shape of a 1 µm x 10 µm wire, with 2 µm x 3 µm contact pads at each end of the wire (U = -2 V, I = 0.02 nA, depassivation parameters: U_{lith} = 8 V, I = 2 pA, 100 nm/s). Note c) is a higher resolution image of the area highlighted in b). d)-e) Surface after exposure to a saturation dose of 0.03 Langmuir of PH_3, showing that PH_3 adsorption occurs exclusively in the depassivated region in d). e) shows a magnified area of this region.

STM imaging is challenging due to unstable tunnel conditions resulting from loosely attached PH_3 molecules in the tunnel junction. To minimise the risk of contaminating the patterned area with material from the tip, induced by PH_3 tip modifications, only a few low resolution images were acquired directly after dosing.

Kelvin probe force microscope

The Kelvin probe force microscope (KPFM), firstly introduced by Nonnenmacher et al.,[1] is based on a non-contact variant AFM setup and detects the contact potential difference V_{CPD} between tip and the sample, which originates from their difference in work functions. Whilst scanning, a bias voltage equal to V_{CPD} is applied to compensate for induced local electrostatic forces F_{ES}. In addition to the DC bias, an AC bias well below the AFM cantilever resonance frequency is added and applied between tip and sample, yielding

$$V = (V_{DC} - V_{CPD}) + V_{AC} sin(\omega t)\,. \qquad (1)$$

The AC component of the applied voltage will cause the cantilever to vibrate and a lock-in amplifier is used to detect the changes of the cantilever oscillation around ω. The resulting vibration of the cantilever is detected using a diode laser and a four-quadrant detector, depicted in Figure 1 (main text). The electrostatic

force F_{ES} in a capacitor (were the plates of the capacitor here represent an AFM tip and a buried conducting region in the device) is found by differentiating the energy function with respect to the tip-sample separation z,[2,3] resulting in

$$F_{ES} = \frac{1}{2}\frac{\partial C}{dz}V^2, \qquad (2)$$

where C is the capacitance and V is the voltage applied between tip and surface. By substituting the previous formula (1) for the applied voltage in Equation (2), the electrostatic force can be split up into three spectral component contributions:

$$F = F_{DC} + F_{\omega} + F_{2\omega}. \qquad (3)$$

The force acting on the cantilever can be split into a static (F_{DC}) and dynamic contributions (F_{ω},$F_{2\omega}$) given as

$$F_{DC} = \frac{1}{2}\frac{\partial C}{dz}[(V_{DC} - V_{CPD})^2 + \frac{1}{2}V_{AC}^2] \qquad (4)$$

$$F_{\omega} = \frac{\partial C}{dz}[V_{DC} - V_{CPD}]V_{AC}sin(\omega t) \qquad (5)$$

$$F_{2\omega} = \frac{1}{4}\frac{\partial C}{dz}V_{AC}^2 cos(2\omega t) \qquad (6)$$

For contact potential measurements the electrostatic force F_{ω} is nullified by applying a DC potential at the tip that exactly compensates the total potential Φ_{total} comprising of $\Phi_{total} = V_{CPD} - V$,[4] where V is the applied SD bias and V_{CPD} is the contact potential difference originating from the local work function difference of tip and sample. A feedback loop is used to maintain $F_{\omega} = 0$ in conjunction with the lock-in amplifier that detects the cantilever oscillation at ω. Φ_{total} is acquired as an image and thus the local potential of the surface is probed as an 'electronic potential map' as function of SD bias.

KPFM has been employed to image p-type dopant profiles[5] and individual P dopants[6,7,8] and clusters[9] at the surface of a P-doped silicon-on-insulator-field-effect-transistor (SOI-FET) channel at low temperatures (≈13 K). We use the conventional KPFM operation mode at room temperature where the AC bias is applied between tip and sample and a DC bias is applied between S and D by only varying the potential on the top source electrode while the drain electrode is set to ground. This way KPFM probes the local change in total potential Φ_{total}.

The potential landscape of the active device

For U = -1.3 V the bias application is clearly reflected in the surface potential image shown in Figure S3a revealing a large negative electronic potential increase on the top S contact, the metallic contamination (MC), and the silicon in close proximation to the top contact. A more negative electric potential is associated with the presence of positive charges such as holes and/or depleted dopants while a more positive electric potential can be associated with negative charges (electrons), respectively.[10] We note that the potential response to changes in S and D bias of the circular protrusion is similar to those of the Al contacts, pointing towards a metallic contamination (MC) as mentioned earlier.

The bottom drain contact is set to ground and as expected most of the absolute potential variations occur at the top S contact as visualised in a potential map in Figure S3b. The detected total surface potential difference between S and D (black and red circles as indicated in Figure S3a) is plotted against the actual applied voltage in Figure S3c which reveals that the detected surface potential difference (blue curve) approximately follows an ideal ohmic behaviour (green curve, plotted with determined V_{CPD}). From this, we can conclude that the applied bias voltage drops uniformly between the S and D contacts, confirming the fabrication of high-quality electric contacts to the buried wire. We can determine the contact potential difference of our PtSi tip and the Al contact from the flatband voltage at V = 0 V of the blue curve and/or the average offset between green and blue curve as V_{CPD}(PtSi/AL) = (0.36±0.03) V. This is an important result as it deviates strongly from the calculated work function difference between PtSi and Al of V_{CPD}(PtSi/AL) = $W_{PtSi} - W_{Al}$ = 4.97V - 4.28V ≈ 0.7 V.[5,11]

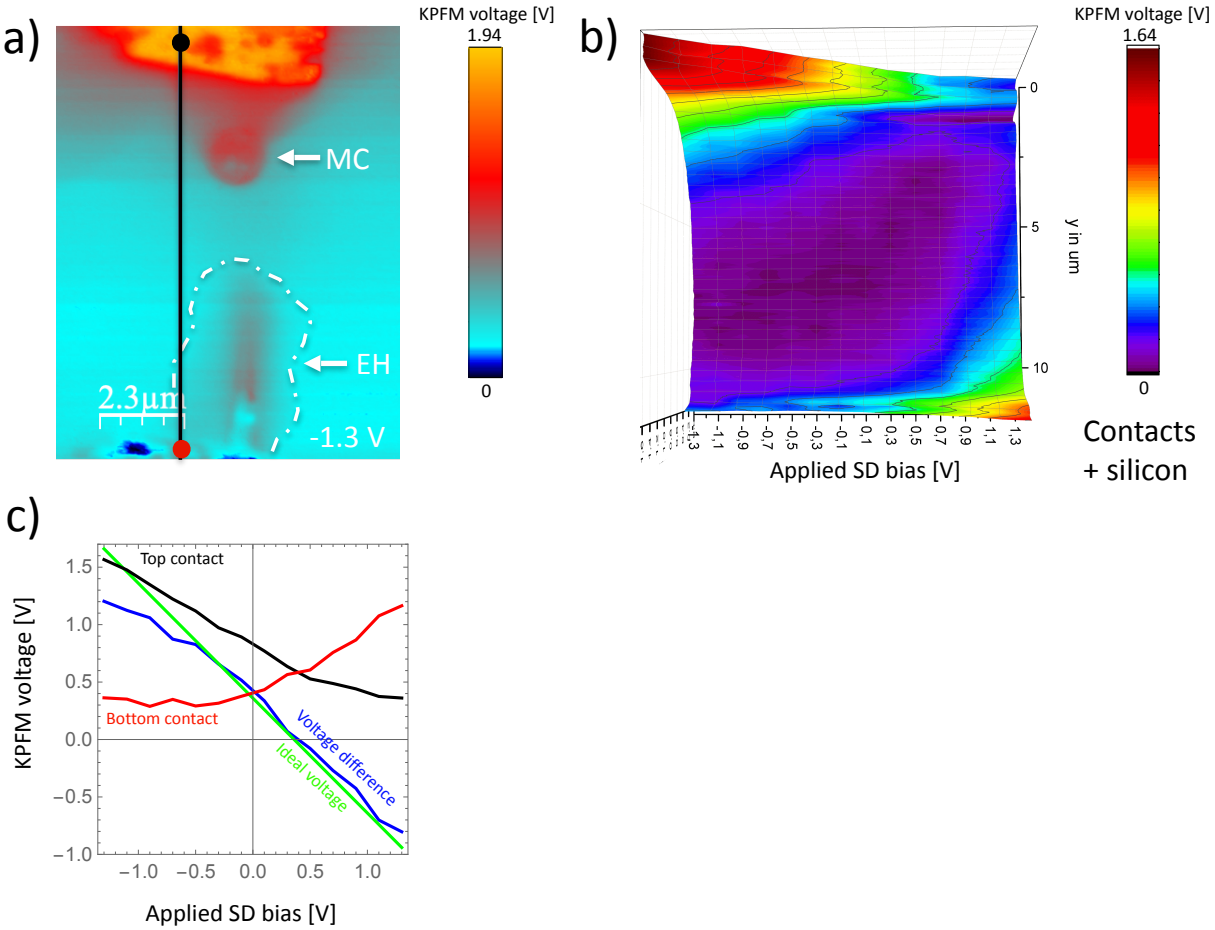

Figure S3: a) KPFM surface potential image obtained at -1.3 V of the buried P-wire region plus S and D Al contacts. The vertical line indicates the location of an obtained surface potential slide as a function of applied bias plotted as 3D graph in b). The black and red circle mark the points at the top and bottom electrode, respectively that are plotted in c) as a function of applied bias together with their difference (blue) and the ideal voltage offset including the contact potential difference of 0.36 V. The arrows indicate presence of metallic contamination (MC) and epitaxial hole (EH) while the dotted line highlights the perimeter of the epitaxial hole region.

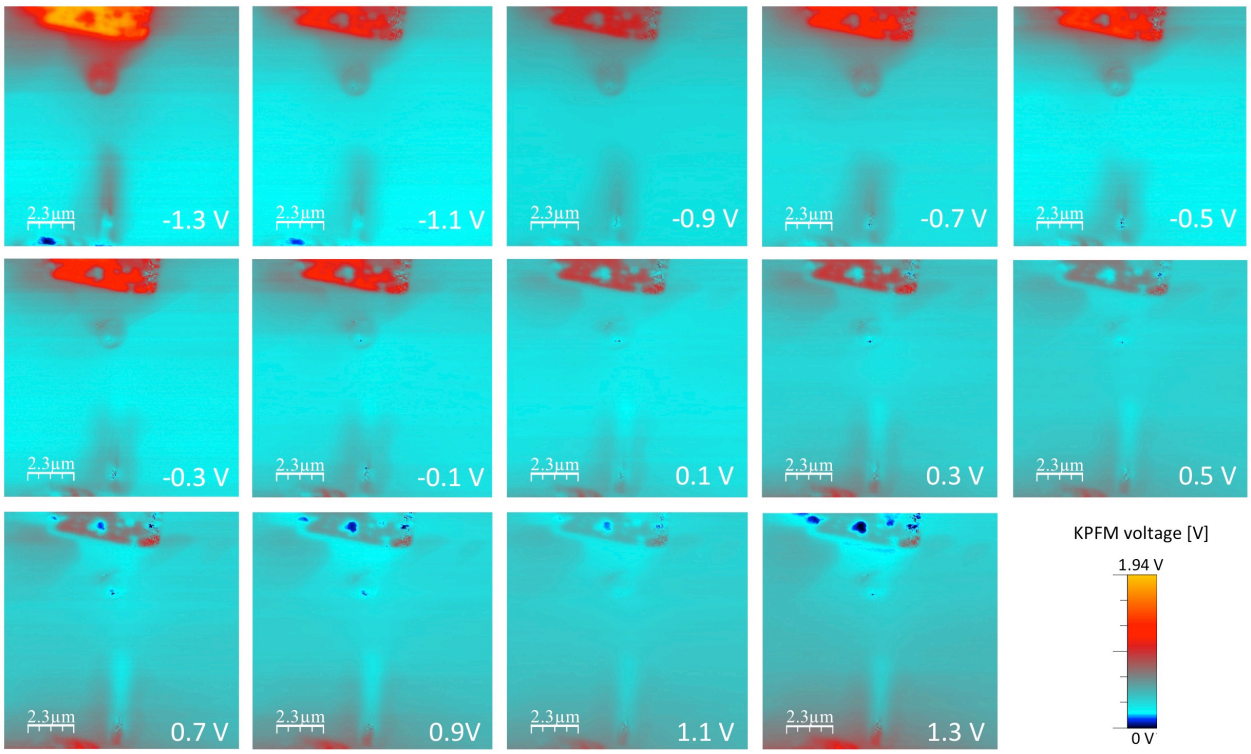

Figure S4: KPFM electronic surface potential images of the buried P wire device plus Al contact for SD bias voltages between -1.3 V to 1.3 V. Scale 11.6 µm x 11.6 µm. The main contrast is arising from the regions of the SD Al contacts.

The complete data set of Kelvin probe force microscopy (KPFM) surface potential images obtained from -1.3 V to +1.3 V SD bias that form the basis for the surface potential maps in FigureS3b are presented in Figure S4. Note that the contrast is adjusted to visualise the maximal potential difference of the device. Since the surface resembles feature heights of up to 200 nm cross correlation of the KPFM potential to the topography need to be considered when comparing potentials of different locations on the sample to each other. For the spectra acquired on the contacts in Figure S3c no cross correlation to the topography has been detected since both contacts reside on roughly the same height level.

Scanning Capacitance Force Microscopy

The following section is summarised form reference[3]. The ∂C/∂z component in the $F_{2\omega}$ signal could be measured directly by a lock-in detection of the second harmonic oscillation but is not commonly used because it contains topographic artefacts.

The basic idea of scanning capacitance force microscopy (SCFM) is to detect an induced electrostatic force oscillating at the third harmonic frequency 3ω of the cantilever. ∂C/∂z also depends on the applied bias voltage and hence ∂C(V,z)/∂z is composed of a DC and AC component, approximated as

$$\frac{\partial C(V,z)}{\partial z} \simeq \frac{\partial C(V_{DC},z)}{\partial z} + \frac{\partial C(V_{DC},z)}{\partial V \partial z} V_{AC} cos(\omega t)\,. \qquad (7)$$

Accordingly, F_{ES} contains a force component that oscillates at 3ω of the electrical excitation frequency, given as

$$F_{3\omega} \simeq \frac{1}{8} \frac{\partial^2 C(V_{DC},z)}{\partial V \partial z} V_{AC}^3 cos(3\omega t)\,. \qquad (8)$$

Hence, the detected amplitude $A_{3\omega}$ of the third harmonic oscillation is related to the voltage derivative of the force gradient by

$$A_{3\omega} \propto \frac{\partial^2 C(V_{DC},z)}{\partial V \partial z} V_{AC}^3 cos(3\omega t). \qquad (9)$$

The full set of SCFM ∂C/∂V amplitude images obtained at varying SD bias voltages ranging from -1.8 V to 1.8 V shown in 3D maps in Figure 3 is presented in Figure S5.

Model the IV characteristic of the P-wire device

We apply a model from Grillo et al.[12] to our measured device IV which has been developed to describe the conduction in a two-terminal silicon device with two Schottky junctions at the contacts. First, by subtracting the ohmic IV function of the P-wire (shown in Figure 3a) which is obtained from a linear fit between -0.5 V and 0.5 V from the measured IV of our P-wire device allows to obtain the IV characteristic of the back-to-back Al-silicon Schottky contact channel without the wire IV contribution (black curve in Figure S6).

Following[12], the total current I_T can be modelled as

$$I_T = \frac{2 I_{S1} I_{S2} sinh(\frac{qV}{2kT})}{I_{S1} e^{(\frac{qV}{2kT})} + I_{S2} e^{(\frac{-qV}{2kT})}} \qquad (10)$$

where

$$I_{S1,S2} = S_{1,2} A^* T^2 exp(\frac{-\Phi_{B1,B2}}{kT}) \qquad (11)$$

is the reverse saturation currents, *A** is the Richardson constant, *T* is the temperature, *k* is the Boltzmann constant, and $S_{1,2}$ are the areas of the junctions. To allow for a slight deviation of the barrier heights from the ideal case, the effective Schottky barriers Φ_{B_1,B_2} can be written as

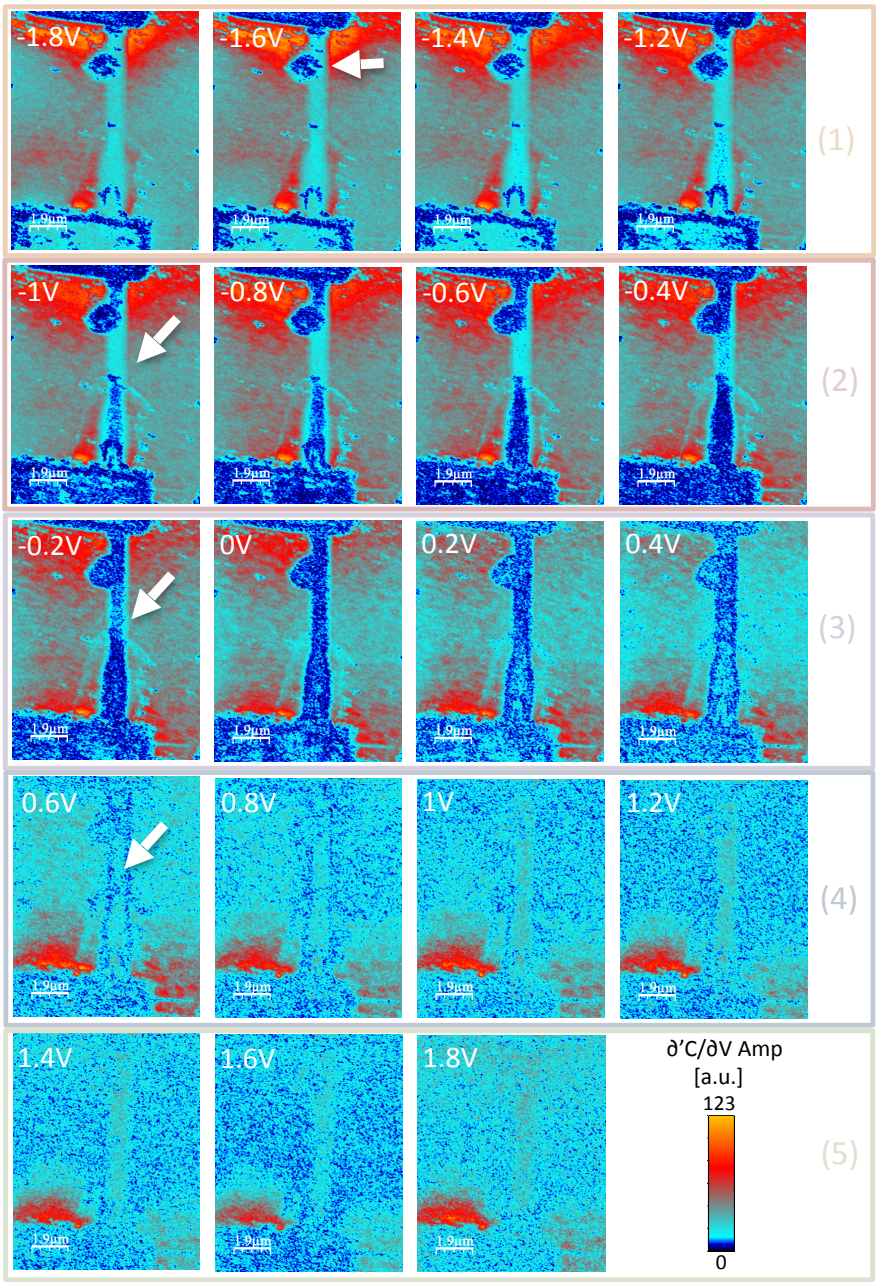

Figure S5: Set of 19 SCFM ∂C/∂V amplitude images (12mm x 9mm) of the buried P wire region plus Al contact obtained for SD bias voltages from -1.8 V to 1.8 V. Applied AC voltage of 1.7 V at 15 kHz.

$$\Phi_{B_1,B_2} = \Phi_{B_{01},B_{02}} \pm eV_{1,2}(1 - \frac{1}{n_{1,2}}) \qquad (12)$$

where $\Phi_{B_{01},B_{02}}$ are the ideal Schottky barriers at zero bias, V_1 and V_2 are the voltage drops at the junctions and $n_{1,2}$ are the ideality factors defined as

$$\frac{1}{n_{1,2}} = 1 \pm \frac{\partial \Phi_{B_1,B_2}}{e\,\partial V_{1,2}}. \qquad (13)$$

Comparing the simulated total current I_T for varying $n_{1,2}$ and $\Phi_{B_{01},B_{02}}$ to our IV characteristic of the back-to-back Al-silicon Schottky contact channel allows to understand the evolution from an expected "ideal IV" to our measured device IV. Note that for all simulated I_T curves we assume a constant area of both contacts $S_1 = S_2 = 1$ and $T = 300$ K. We also make a simplifying assumption of $V_1 = V_2 = V/2$.

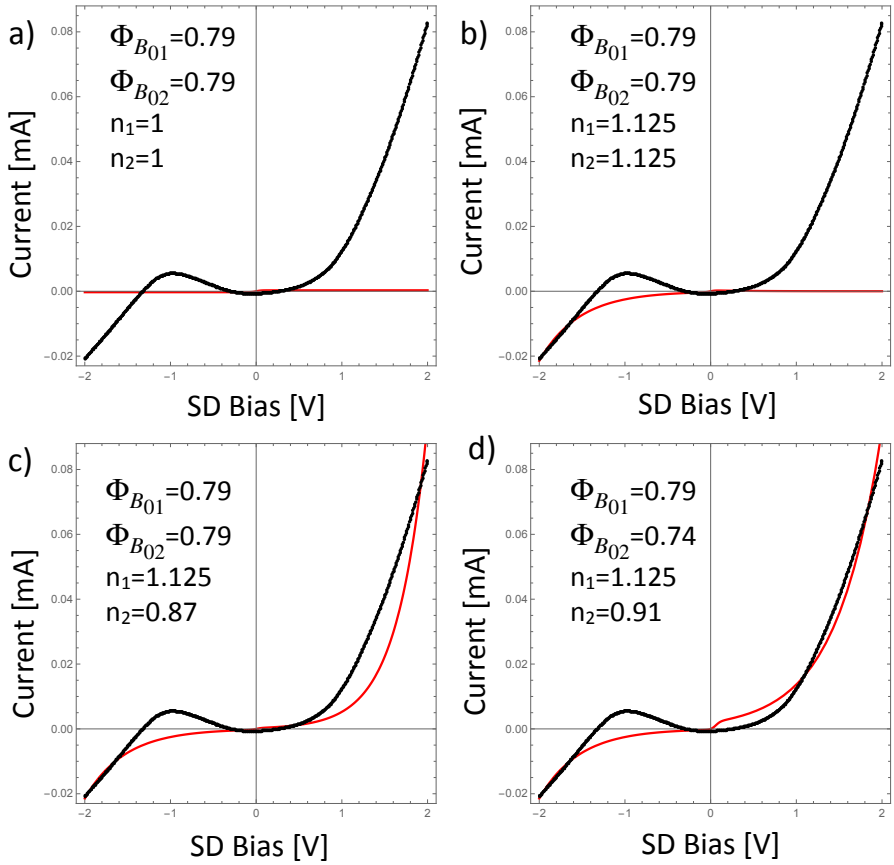

Figure S6: Model of the back-to-back Al-silicon Schottky contact IV characteristic following[12]. Comparing the simulated total current I_T (red curve) for varying barrier heights $\Phi_{B_{01},B_{02}}$ and ideality factors $n_{1,2}$ to the IV characteristic of the back-to-back Al-silicon Schottky contact channel.

Figure S6a displays the modelled IV (red curve) using Equation (10) for a two contact device comprising an equal barrier height of $\Phi_{B_{01}} = \Phi_{B_{02}} = 0.79$ V with no deviation from the ideal case ($n_{1,2} = 0$), which doesn't compare well to the measured current level of the back-to-back Al-silicon Schottky contact IV (black curve). Only by allowing a slight deviation from the ideal scenario for both barrier sides, $n_1 = 1.125$ for negative voltes (see Figure S6b) and $n_2 = 0.87$ for positive voltages (see Figure S6c), the simulated I_T curve matches the measured IV for both SD bias directions. The best estimation includes a slightly varying barrier height of $\Phi_{B_{02}} = 0.74$ V and an ideality factor of $n_2 = 0.91$ (see Figure S6d).

We conclude that the applied model provides a reasonable fit to the back-to-back Al-silicon Schottky contact channel IV by estimating only a small deviation from the ideal case and barrier heights of $\Phi_{B_{01}} = 0.79$ V and $\Phi_{B_{02}} = 0.74$ V. The deviation to the ideal case are probably the result of trapped charges, defects, inadvertent oxide layers, and/or image-force lowering that make the SB height dependent on the applied external voltage[12].

Dynamic SMM spectroscopy

To minimize the surface stress during measurements at high voltages in contact mode, we acquire the spectroscopy data dynamically by keeping the *y*-scan direction fixed and gradually sweeping the DC bias whilst scanning in *x*-direction (dashed line scan indicated in Figure S7a). An average of several vertical lines in the obtained dS_{11}/dV amplitude and phase voltage line scan maps provide information equivalent to those obtained from standard point spectroscopy. A vertical line in these maps represents a spectra for an individual location on the sample as shown in part 2 of Figure S7. After the calibration procedure quantitative spectroscopy curves are obtained. (Compare part 3 in Figure S7).

The spectroscopy data shown in Figure S7 obtained on silicon (blue) and the unperturbed wire region (purple) in *y*-modulation allows to quantitatively determine the selective wire contribution to the overall local

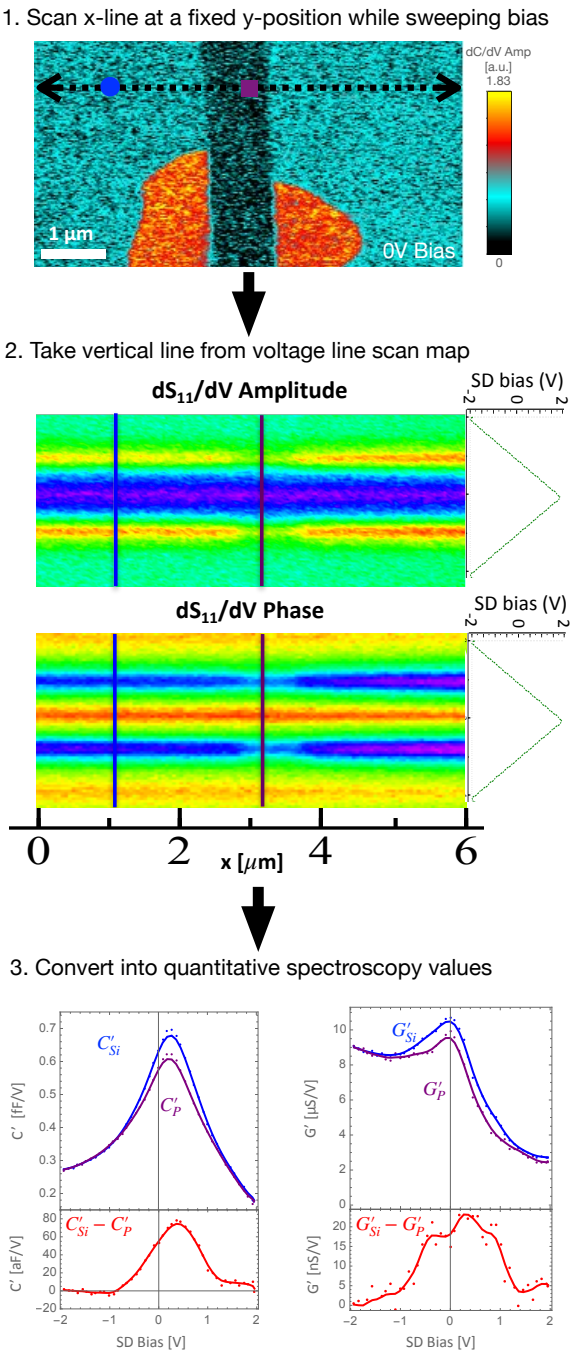

Figure S7: Spectroscopy data acquired dynamically by (1) keeping the *x*-scan direction fixed and gradually sweeping the DC bias whilst scanning (scan line indicated). An average of several vertical lines in the obtained voltage line scan map (2) provides information equivalent to those obtained from standard point spectroscopy. After calibration (3) quantitative point spectroscopy data is obtained.

change in capacitance and conductance as it would be highly desirable for a device showing no imperfections.

References

1. Nonnenmacher, M., M. P. o'Boyle, and H. Kumar Wickramasinghe. "Kelvin probe force microscopy." Applied physics letters 58.25 (1991): 2921-2923.
2. Martin, Yves, David W. Abraham, and H. Kumar Wickramasinghe. "High-resolution capacitance measurement and potentiometry by force microscopy." Applied Physics Letters 52.13 (1988): 1103-1105.
3. Kobayashi, Kei, Hirofumi Yamada, and Kazumi Matsushige. "Dopant profiling on semiconducting sample by scanning capacitance force microscopy." Applied physics letters 81.14 (2002): 2629-2631.
4. S. M. Sze and K. K. Ng, Physics of semiconductor devices. Wiley-Interscience, 2007.
5. Gysin, U., et al. "Dopant imaging of power semiconductor device cross sections." Microelectronic Engineering 160 (2016): 18-21.
6. Anwar, Miftahul, et al. "Single-electron charging in phosphorus donors in silicon observed by low-temperature Kelvin probe force microscope." Japanese Journal of Applied Physics 50.8S3 (2011): 08LB10.
7. Ligowski, Maciej, et al. "Observation of individual dopants in a thin silicon layer by low temperature Kelvin Probe Force Microscope." Applied Physics Letters 93.14 (2008): 142101.
8. Moraru, Daniel, et al. "Atom devices based on single dopants in silicon nanostructures." Nanoscale research letters 6.1 (2011): 479.
9. Moraru, Daniel, et al. "Tunneling in systems of coupled dopant-atoms in silicon nano-devices." Nanoscale research letters 10.1 (2015): 372.
10. Tyszka, K., et al. "Comparative study of donor-induced quantum dots in Si nano-channels by single-electron transport characterization and Kelvin probe force microscopy." Journal of Applied Physics 117.24 (2015): 244307.
11. Giannazzo, Filippo, et al. "Conductive atomic force microscopy of semiconducting transition metal dichalcogenides and heterostructures." *Nanomaterials* 10.4 (2020): 803.
12. Grillo, Alessandro, and Antonio Di Bartolomeo. "A current–voltage model for double Schottky barrier devices." *Advanced Electronic Materials* 7.2 (2021): 2000979.